

Thioperoxy Derivative Generated by UV-Induced Transformation of *N*-Hydroxypyridine-2(1*H*)-thione Isolated in Low-Temperature Matrixes

Leszek Lapinski, Anna Gerega, Andrzej L. Sobolewski, and Maciej J. Nowak*

Institute of Physics, Polish Academy of Sciences, Al. Lotnikow 32/46, 02-668 Warsaw, Poland

Received: September 13, 2007; In Final Form: October 15, 2007

Photochemical transformations of *N*-hydroxypyridine-2(1*H*)-thione and its deuterated isotopologue were studied using the matrix-isolation technique. Low-temperature Ar and N₂ matrixes containing monomers of this compound were irradiated with continuous-wave near-UV light. Photogeneration of two products was observed in these experiments. The relative population of these photogenerated species was found to be dependent on the wavelength of the UV light used for irradiation. By comparison of the IR spectra of the photoproducts with the spectra simulated theoretically at the DFT(B3LYP)/6-311++G(d, p) level, the final and the intermediate products were identified as rotameric forms of 2-hydroxysulfanyl-pyridine. This is the first report on generation of this thioperoxy derivative of pyridine. The mechanism of photogeneration of 2-hydroxysulfanyl-pyridine involves a photoinduced cleavage of the N–O bond in *N*-hydroxypyridine-2(1*H*)-thione, generation of the •OH radical weakly bound with the remaining pyridylthiyl radical, and recombination of these two radicals by formation of the new –S–O– bond. A theoretical model supporting this interpretation was constructed on the basis of approximate coupled cluster (CC2) calculations of the potential energy surfaces of the ground and first excited singlet electronic states of the system. After electronic excitation of the monomeric *N*-hydroxypyridine-2(1*H*)-thione, the molecule evolves to the conical intersection with the potential energy surface of the ground state and then to the global minimum corresponding to 2-hydroxysulfanyl-pyridine.

Introduction

N-Hydroxypyridine-2(1*H*)-thione is a commercial substance (called also omadine or pyrithione) known for its antibacterial, anticancer, antifungal, and antidandruff activities.^{1–4} This compound received also a significant attention as a candidate for a good photochemical precursor of hydroxyl radicals (•OH).

DNA damage induced by hydroxyl radicals is an occurrence recognized on the basis of numerous experimental investigations.^{5–7} Interaction with hydroxyl radicals was demonstrated to generate single-strand breaks in polynucleotide chains as well as modifications of nucleic acid bases. Recently, it was suggested that •OH radicals can play a key role in oxidation of guanine to 8-oxo-7,8-dihydroguanine.⁸ Hence, hydroxyl radicals give rise to oxidative modifications and mutations which can initiate carcinogenesis or/and a series of age-correlated degenerative diseases.

For the sake of experimental investigation of interactions of hydroxyl radicals with nucleic acids constituents, the method of in situ generation of •OH radicals is of crucial importance. In comparison with chemical formation of such radicals (through the Fenton reaction⁹), many advantages are offered by photochemical methods based on light-induced decomposition of precursors (photo-Fenton reagents). It is important to use precursors that would allow photogeneration of •OH radicals in a specific way (without inducing other photoreactions accompanying production of hydroxyl radicals). The ideal precursor should also release •OH radical under mild irradiation conditions (using long-wavelength light that would not directly excite nucleic acids constituents).

N-Hydroxypyridine-2(1*H*)-thione has been used as a photochemical source of •OH radicals in a number of studies on oxidative damage of DNA.^{10–13} This species absorbs at wavelengths as long as 400 nm.¹⁴ It was observed that hydroxyl radicals were photogenerated from *N*-hydroxypyridine-2(1*H*)-thione upon UV ($\lambda > 350$ nm) irradiation. These mild photochemical conditions constitute an obvious advantage of *N*-hydroxypyridine-2(1*H*)-thione as a precursor. On the other hand, Aveline and co-workers^{14–16} claimed that *N*-hydroxypyridine-2(1*H*)-thione was a nonspecific hydroxyl radical generator. This conclusion, however, was based on investigations carried out with pulsed sources of light (pulse duration 8 ns). Hence, successive absorption of two photons, quite probable to occur for a thione compound, might be responsible for photogeneration of multiple species upon ($\lambda = 355$ nm) pulsed irradiation of *N*-hydroxypyridine-2(1*H*)-thione.

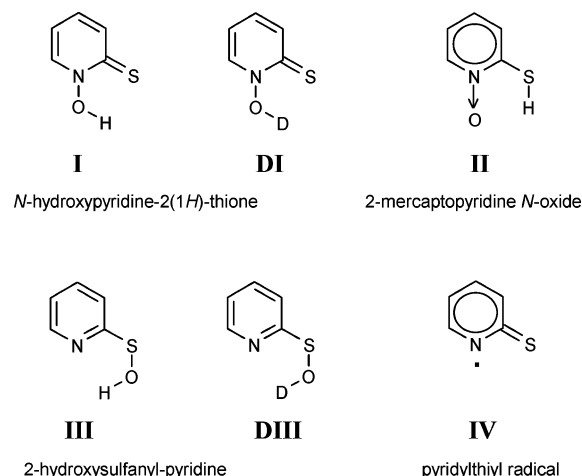
The experiments carried out within the present work concern monomers of *N*-hydroxypyridine-2(1*H*)-thione isolated in low-temperature Ar and N₂ matrixes. The objective of the current study focuses on phototransformations of this compound induced by irradiation with continuous-wave UV light. This approach led to analyzable results. The interpretation of the observed photochemical phenomena was aided by theoretical calculations using the methods of quantum chemistry.

Experimental Section

The sample of *N*-hydroxypyridine-2(1*H*)-thione used in the present study was supplied by Aldrich (2-mercaptopyridine-1-oxide, CAS: 1121-31-9). The isotopologue with the labile hydrogen atom replaced by deuterium was prepared by two cycles of dissolving in deuterated methanol (99% D, Aldrich)

* To whom correspondence should be addressed. E-mail: mjinow@ifpan.edu.pl.

CHART 1: Structures of *N*-Hydroxypyridine-2(1*H*)-thione Isomers, Isotopologues, and Pyridylthiyl Radical



or deuterated ethanol (99.5% D, Aldrich) and drying in a stream of clean, gaseous nitrogen coming from above liquid N₂. The solid compound was placed in a glass tube connected to the vacuum chamber of a continuous-flow helium cryostat through a regulating valve. Even at room temperature the saturated vapor pressure over the solid compound is sufficient for deposition of the matrixes. The vapors of the *N*-hydroxypyridine-2(1*H*)-thione (typically at 24 °C) were deposited, together with a large excess of inert gas (argon or nitrogen), on a CsI window cooled to 10 K. The argon and nitrogen matrix gases were of spectral purity, as supplied by Linde AG and Technische Gase, Leipzig. The IR spectra were recorded with 0.5 cm⁻¹ resolution using the Thermo Nicolet Nexus 670 FTIR spectrometer equipped with a KBr or a “solid substrate” beam splitter and DTGS detectors. Intensities of the IR absorption bands were measured by numerical integration. Matrixes were irradiated with light from an HBO200 high-pressure mercury lamp fitted with a water filter and an appropriate cutoff filter. In order to study dependence of investigated photoprocesses on the wavelength of the UV light used for irradiation, the following cutoff filters were applied: WG295, WG345, or GG13/2 transmitting light with $\lambda > 295$ nm, $\lambda > 345$ nm, or $\lambda > 385$ nm, respectively.

Computational Section

The geometries of *N*-hydroxypyridine-2(1*H*)-thione isomers (presented in Chart 1 and Table 1) were fully optimized using the MP2 method¹⁷ as well as using the hybrid Hartree–Fock and density functional theory method DFT(B3LYP) with the Becke’s three-parameter exchange functional¹⁸ and gradient-corrected functional of Lee, Yang, and Parr.¹⁹ At the MP2 calculated equilibrium geometries the relative energies of these forms were computed at the same level of theory. At DFT-(B3LYP) optimized geometries the electronic energies were computed also at the QCISD level.²⁰ The resulting relative energies of isomeric forms *N*-hydroxypyridine-2(1*H*)-thione are collected in Table 1 and in Table S1 (Supporting Information). It is commonly known that although the MP2 method provides more reliable values of relative electronic energies, it reproduces the infrared spectra somewhat less accurately than the DFT calculations. That is why the harmonic vibrational frequencies and IR intensities were calculated using the DFT(B3LYP) method at the geometries optimized at the same level of theory. In calculations concerning pyridylthiyl radical **IV** (formed by cleavage of hydroxyl radical from *N*-hydroxypyridine-2(1*H*)-

thione) the multiplicity 2 (doublet) was used. All quantum-mechanical calculations, concerning the ground electronic state, were performed with the Gaussian 03 program²¹ using the 6-311++G(d, p) or 6-31++G(d, p) basis sets. To correct for the systematic shortcomings of the applied methodology (mainly for anharmonicity), the predicted vibrational wavenumbers were scaled down by a single factor of 0.98. The theoretical normal modes were analyzed by carrying out the potential energy distribution (PED) calculations. Transformations of the force constants with respect to the Cartesian coordinates to the force constants with respect to the molecule fixed internal coordinates allowed the normal-coordinate analysis to be performed as described by Schachtschneider.²² The internal coordinates used in this analysis were defined following the recommendations of Pulay et al.²³ These coordinates are listed in Table S2 (Supporting Information). Potential energy distribution matrices²⁴ have been calculated, and the elements of these matrices greater than 10% are given in Tables S3–S8 (Supporting Information).

Energy differences between S₀ and the lowest excited electronic states were calculated, for structures **I** and **IIIa**, at geometries optimized for the electronic ground state using the approximate coupled cluster (CC2) method^{25,26} and the Dunning’s correlation-consistent aug-cc-pVDZ basis set.²⁷ For **I** and **IIIa**, equilibrium geometries in S₁ were determined with the CC2 method, making use of the recently implemented CC2 analytic gradients.^{28,29} The cc-pVDZ basis set was used in these geometry optimizations.

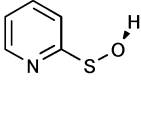
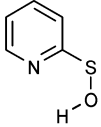
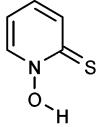
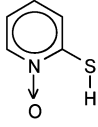
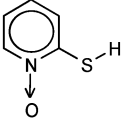
The minimum-energy reaction path for detachment of the hydroxyl group from *N*-hydroxypyridine-2(1*H*)-thione (**I**) in its lowest excited singlet state S₁ was studied with the aid of the CC2 method. The distance between the N and the O atoms was chosen as the driving coordinate for the reaction. All other nuclear degrees of freedom have been optimized for a given value of the driving coordinate. To allow cost-effective explorations of the excited-state potential energy functions, the standard split-valence double- ζ basis set with polarization functions on heavy atoms (def-SV(P))³⁰ has been employed in the optimizations of geometries of the points along the reaction path. At the optimized geometries along the determined reaction path, single-point energy calculations were executed with the CC2/cc-pVDZ method. An analogous method was employed for the study of the hydroxyl group detachment (by cleavage of the SO bond) or attachment (by formation of the SO bond) in **IIIa**.

All the CC2 calculations were performed with the aid of the Turbomole program package²⁶ making use of the resolution-of-the-identity (RI) approximation for the evaluation of the electron-repulsion integrals.

Experimental Results

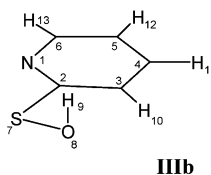
N-Hydroxypyridine-2(1*H*)-thione is also referred to as 2-mercaptopyridine *N*-oxide. These two names correspond to structures **I** and **II**, respectively (see Chart 1). The possibility of the molecule to adopt structures **I** and **II**, differing only by the position of the labile hydrogen atom, makes the case an example of prototropic tautomerism. Hence, for the compound in the gas phase, an equilibrium reflecting (in terms of Boltzmann’s distribution) relative stabilities of forms **I** and **II** should be expected. In the current work, relative energies of forms **I** and **II** were calculated at the MP2/6-311++G(d, p) and QCISD/6-31++G(d, p) levels. The results of these calculations are presented in Table 1. The *N*-hydroxy form **I** was predicted to be substantially more stable (by ca. 30 kJ mol⁻¹) than the *N*-oxide form **IIa**. Crystallographic investigation by Bond and

TABLE 1: Relative Electronic (ΔE_{el}), Zero-Point Vibrational (ΔZPE), and Total ($\Delta E_{el} + \Delta ZPE$) Energies (kJ mol^{-1}) of *N*-Hydroxypyridine-2(1*H*)-thione Isomers^a

					
	IIIb	IIIa	I	IIa	IIb
$\Delta E_{el}(\text{DFT})$	-53.8	-56.4	0.0	28.5	42.0
$\Delta ZPE(\text{DFT})$	2.7	2.9	0.0	8.0	6.8
$\Delta E_{el}(\text{DFT})+\Delta ZPE(\text{DFT})$	-51.1	-53.5	0.0	36.5	48.8
$\Delta E_{el}(\text{MP2})$	-66.7	-66.9 †	0.0	21.1	31.9
$\Delta E_{el}(\text{MP2})+\Delta ZPE(\text{DFT})$	-64.0	-64.0	0.0	29.1	38.7
$\Delta E_{el}(\text{QCISD})\ddagger$	-85.0	-81.6	0.0	24.8	35.3
$\Delta E_{el}(\text{QCISD})\ddagger+\Delta ZPE(\text{DFT})$	-82.3	-78.7	0.0	32.8	42.1

† Nonplanar structure, torsion angles: $\tau(\text{HOSC})=55.7^\circ$, $\tau(\text{OSCN})=32.5^\circ$

‡ QCISD calculations were carried out using the 6-31++G(d,p) basis set at geometry optimized at the DFT(B3LYP)/6-311++G(d,p) level.



$$\beta(\text{H9-O8-S7}) = 106.9^\circ$$

$$\beta(\text{O8-S7-C2}) = 100.3^\circ$$

$$\tau(\text{H9-O8-S7-C2}) = 95.4^\circ$$

$$\tau(\text{O8-S7-C2-N1}) = 169.5^\circ$$

^a The energy of the form **I** was taken as reference. The DFT(B3LYP) and MP2 calculations were carried out using the 6-311++G(d, p) basis set.

Jones demonstrated that in the solid state the compound adopts the *N*-hydroxy-thione form **I**.³¹

For isomer **II**, the energy of its rotameric form **IIIb**, with the SH group rotated by 180°, was also calculated. As could be expected, the energy of this rotamer was predicted to be higher (by ca. 10 kJ mol^{-1} , see Table 1) than the energy of the rotamer **IIa**. The difference in energy reflects stabilization of the latter form by an interaction of the -SH hydrogen atom with the lone electron pair of the $\text{N} \rightarrow \text{O}$ oxygen atom. Due to analogous reasons, form **I** (as it is presented in Chart 1) should be lower in energy with respect to its rotamer with the OH group rotated by 180°. This latter form turned out not to correspond to a minimum on the potential energy surface. Energy minimization by optimization of geometry of this rotamer led to a barrierless convergence to structure **I** presented in Chart 1.

The results presented in Table 1 suggest also that form **III** should be substantially more stable (by ca. 64–82 kJ mol^{-1}) than form **I**. However, *N*-hydroxypyridine-2(1*H*)-thione cannot easily change the configuration of its atoms and adopt form **III**. In fact, though form **III** is built of the same set of atoms as *N*-hydroxypyridine-2(1*H*)-thione, it should be treated as another compound (2-hydroxysulfanyl-pyridine). Transformation of **I** into **III** would involve breaking of the $\text{N}-\text{O}$ bond, which is quite strong in the ground electronic state of *N*-hydroxypyridine-2(1*H*)-thione. Nevertheless, comparison of calculated energies of forms **I** and **III** is interesting and it seems to be important

for the sake of interpretation of experimental occurrences observed in this work (see the discussion further below).

Taking into account the results of the theoretical predictions of relative energies of forms **I** and **II**, one can expect that in the gas phase at moderate temperatures the *N*-hydroxy isomer **I** should strongly dominate. As a consequence, isomer **I** should be the almost exclusively populated form in the low-temperature matrixes prepared by trapping (on the substrate cooled to 10 K) gaseous *N*-hydroxypyridine-2(1*H*)-thione together with large excess of inert Ar or N_2 . The infrared spectrum of monomers of *N*-hydroxypyridine-2(1*H*)-thione isolated in a low-temperature Ar matrix is presented in Figure 1C. The spectrum of the deuterated isotopologue of *N*-hydroxypyridine-2(1*H*)-thione is shown in Figure 1D. These spectra are compared with the spectra theoretically predicted [at the DFT(B3LYP)/6-311++G-(d, p) level] for isomer **I** (Figure 1A) and deuterated form **DI** (Figure 1B). Infrared spectra of *N*-hydroxypyridine-2(1*H*)-thione and its deuterated isotopologue isolated in N_2 matrixes are presented in Figure S1 (in the Supporting Information). The assignment of the IR bands observed in the experimental spectra of *N*-hydroxypyridine-2(1*H*)-thione isolated in low-temperature matrixes to the theoretically calculated normal modes is given in Table S3 (Supporting Information), whereas the analogous assignment concerning the deuterated isotopologue is presented in Table S4 (Supporting Information).

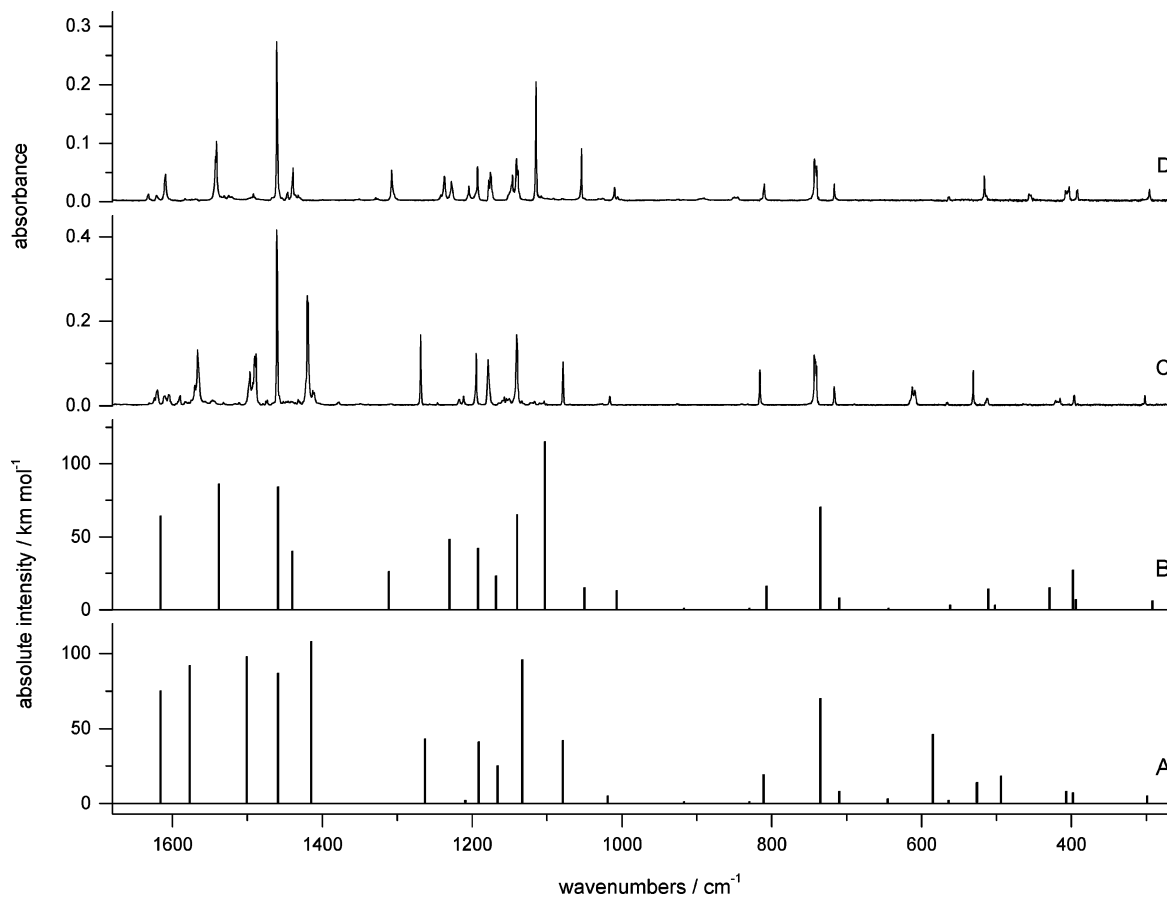


Figure 1. Experimental IR spectra of *N*-hydroxypyridine-2(1*H*)-thione (C) and its deuterated isotopologue (D) isolated in Ar matrixes (10 K), compared with the spectra calculated at the DFT(B3LYP)/6-311++G(d, p) level for form **I** (A) and for deuterated form **DI** (B). The theoretical wavenumbers were scaled by the single factor of 0.98.

The calculated spectrum of 2-mercaptopyridine *N*-oxide (form **II**) reproduces the experimentally recorded spectra of *N*-hydroxypyridine-2(1*H*)-thione slightly less accurately than the spectrum calculated for **I** (Figure S2, Supporting Information). However, the identification of the species isolated in low-temperature matrixes, when based on comparison of experimental spectra with the spectra calculated for **I** and **II**, would not be unambiguous. In this respect, conclusions based on calculations of relative energies of isomers **I** and **II** seem to be much more reliable.

The characteristic feature of the IR spectra of monomeric *N*-hydroxypyridine-2(1*H*)-thione (**I**) is the apparent lack of a well-defined band (see Figure 2) due to the stretching vibration of the OH group (ν OH). For compounds without intramolecular hydrogen bonds,³² such bands are expected in the spectral range of 3650–3550 cm⁻¹. If an intramolecular hydrogen bond (involving an OH group) exists in a molecule, then the ν OH band is significantly shifted toward lower wavenumbers. This effect is accompanied by a substantial broadening of such ν OH band.³² In cases where the hydrogen-bonding interaction is sufficiently strong, the effects described above lead to an apparent disappearance of the ν OH band.³³ The observed IR spectra of monomeric *N*-hydroxypyridine-2(1*H*)-thione demonstrate that the intramolecular –OH⋯S=C hydrogen bonding in **I** is quite a strong interaction leading to a very pronounced broadening and low-wavenumber shift of the ν OH band.

The low-temperature Ar or N₂ matrixes containing monomers of **I** were irradiated with UV light of a high-pressure mercury lamp fitted with a cutoff filter. Upon such irradiation, photogeneration of two products was observed (Figures 2 and 3). The relative yield of these two photoproducts was found to be

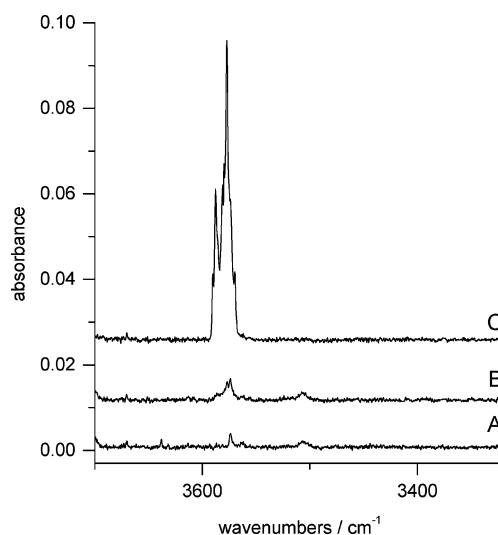


Figure 2. High-frequency region of the infrared spectra of *N*-hydroxypyridine-2(1*H*)-thione isolated in an Ar matrix recorded (A) after deposition of the matrix, (B) after 100 min of UV ($\lambda > 385$ nm) irradiation, and (C) after subsequent 50 min of UV ($\lambda > 345$ nm) irradiation.

dependent on the wavelengths of the light used for irradiation. When the longer-wavelength light was applied ($\lambda > 385$ nm for Ar matrixes), only one of the products was generated (Figure 3B). In the IR spectrum of this species, no sharp band due to ν OH vibration was found (Figure 2B). Instead, a very broad and long-wavelength shifted absorption was observed at ca. 3050 cm⁻¹ (N₂ matrix, see Figure S3 in the Supporting Information). This shows that (similarly to the case of the precursor **I**) also

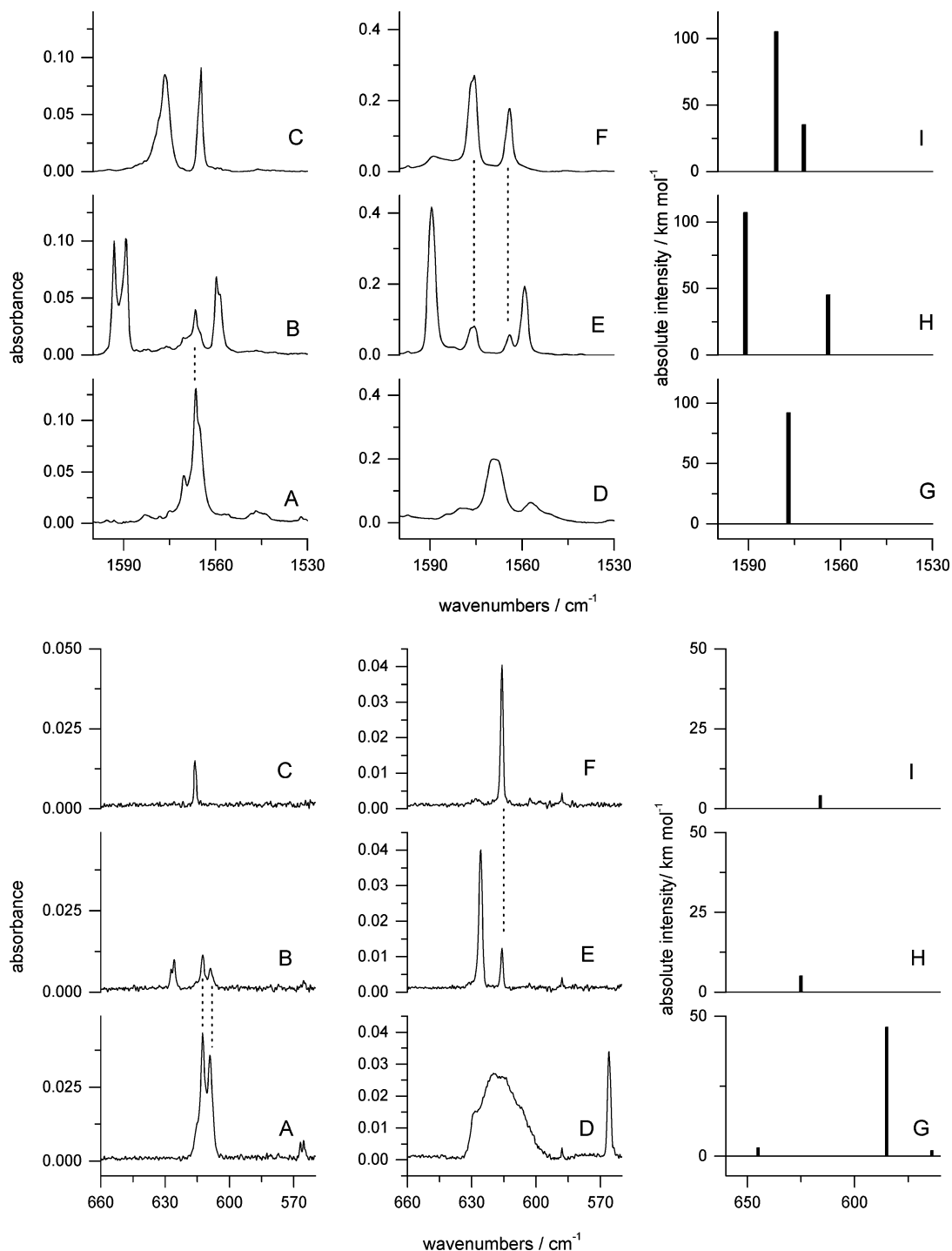


Figure 3. Fragments of the IR spectrum of *N*-hydroxypyridine-2(1*H*)-thione isolated in an Ar matrix: (A) spectrum recorded after deposition of the matrix; (B) spectrum recorded after 100 min of UV ($\lambda > 385$ nm) irradiation; (C) spectrum recorded after subsequent 50 min of UV ($\lambda > 345$ nm) irradiation; corresponding fragments of the IR spectrum of *N*-hydroxypyridine-2(1*H*)-thione isolated in a N₂ matrix; (D) spectrum recorded after deposition of the matrix; (E) spectrum recorded after 15 min of UV ($\lambda > 345$ nm) irradiation; (F) spectrum recorded after subsequent 15 min of UV ($\lambda > 295$ nm) irradiation. Vertical lines indicate bands due to the unreacted initial substrate (Ar matrix) or the final photoproduct (N₂ matrix). Corresponding fragments of the spectra calculated at the DFT(B3LYP)/6-311++G(d, p) level for **I** (G), **IIIa** (H), and **IIIb** (I). The theoretical wavenumbers were scaled by the single factor of 0.98.

in the structure of the photoproduct in question, the OH group interacts with a lone electron pair of a heteroatom.

When the matrixes were irradiated with shorter-wavelength UV light ($\lambda > 345$ nm or $\lambda > 295$ nm) photogeneration of a second product was observed (Figure 3, parts C and F). This was indicated by the appearance of a new spectrum with a characteristic band at 3577 (Ar) or 3566 cm⁻¹ (N₂), see Figure 2C and Figure S3F. Such bands are typical of OH stretching vibrations of OH groups not involved in a hydrogen bond. If a

deuterated isotopologue **DI** was used as a precursor, analogous UV ($\lambda > 345$ nm or $\lambda > 295$ nm) irradiation led to generation of a photoproduct characterized by an IR spectrum (Figure 4) with the band at 2643 (Ar) or 2636 cm⁻¹ (N₂). Such bands are typical of stretching vibrations of a free OD group, not involved in a hydrogen bond.

The experimental observations described above might suggest that upon shorter-wavelength UV ($\lambda > 345$ nm or $\lambda > 295$ nm) irradiation the bond between the OH group and the rest of the

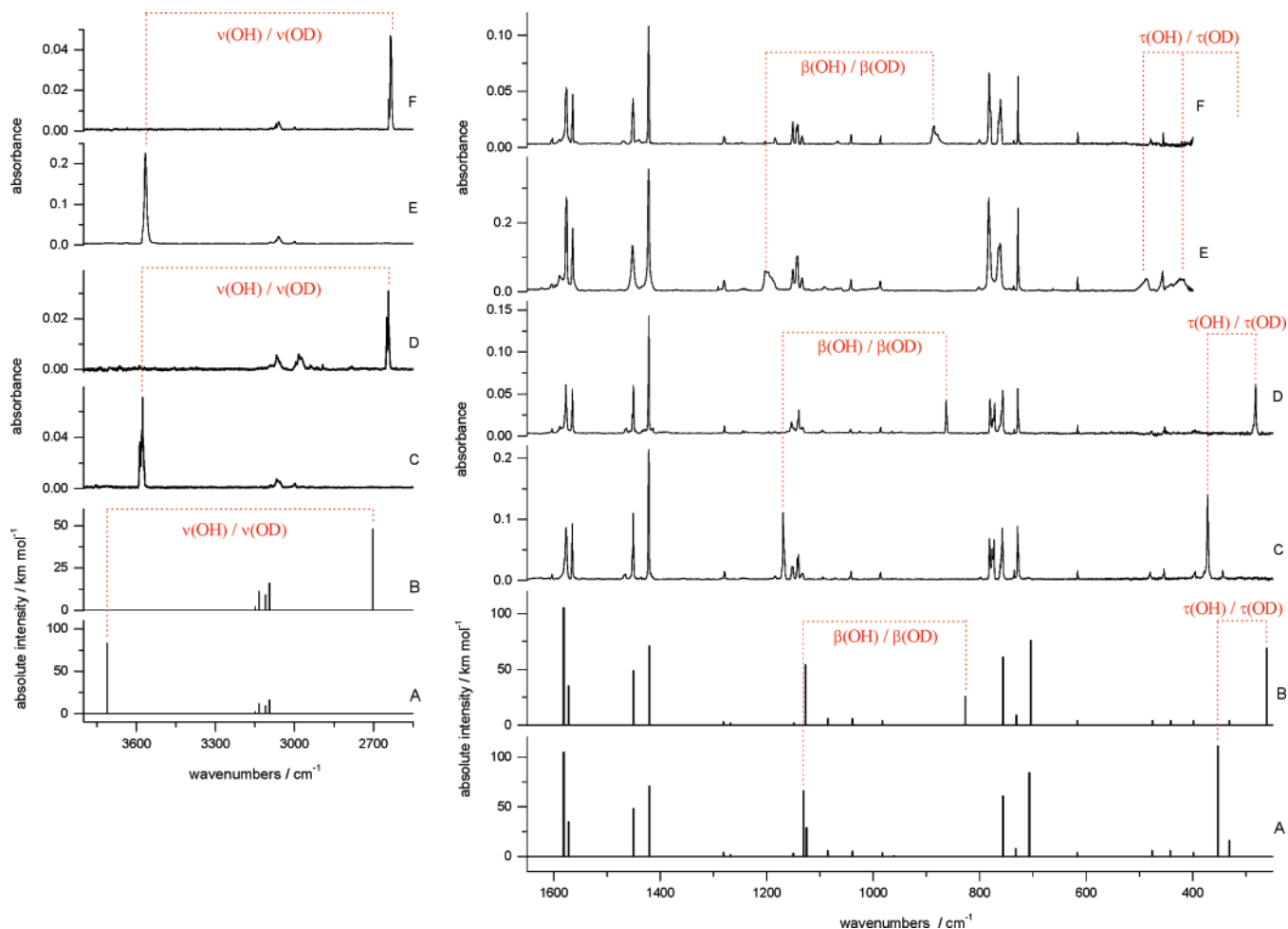


Figure 4. Infrared spectra of the final photoproduct generated upon UV irradiation of *N*-hydroxypyridine-2(1*H*)-thione isolated in an Ar matrix (C) or in a N₂ matrix (E); infrared spectra of the final photoproduct generated upon UV irradiation of the deuterated isotopologue of *N*-hydroxypyridine-2(1*H*)-thione isolated in an Ar matrix (D) or in a N₂ matrix (F); infrared spectra calculated at the DFT(B3LYP)/6-311++G(d, p) level for **IIIb** (A) and **DIIBb** (B). The theoretical wavenumbers were scaled by the single factor of 0.98.

molecule breaks and free $\cdot\text{OH}$ (or $\cdot\text{OD}$) radical is photogenerated. This interpretation would follow the known pattern of photochemical behavior of *N*-hydroxypyridine-2(1*H*)-thione in solutions. Hence, the candidates for the final products of photochemical transformations of matrix-isolated *N*-hydroxypyridine-2(1*H*)-thione would be (1) the hydroxyl radical $\cdot\text{OH}$ or $\cdot\text{OD}$ and (2) the pyridylthiyl radical **IV** (see Chart 1).

A UV-induced process having hydroxyl radical as well as pyridylthiyl radical as final products must involve movement of the smaller fragment outside the matrix cage so that the two radicals are separated in space. This did not seem to be an improbable occurrence. Hydroxyl radicals were previously generated by in situ photolysis of matrix-isolated precursors such as H₂O₂ and HONO.^{34–37} The IR bands due to the stretching vibration of the O–H bond in the $\cdot\text{OH}$ radical were observed at 3554 (Ar),³⁴ 3548 (Ar),³⁸ and 3547 cm⁻¹ (N₂). If $\cdot\text{OH}$ radicals were involved in a hydrogen bond, then the position of the ν OH band was shifted toward lower wavenumbers (significantly lower than 3500 cm⁻¹).³⁵

In comparison to the experimental data collected within the previous works on $\cdot\text{OH}$ radicals generated by in situ photolysis of matrix-isolated precursors,^{34–36} the spectral positions of the ν OH bands observed (within the current work) in the spectra of the final products of UV-induced transformations of *N*-hydroxypyridine-2(1*H*)-thione were considerably higher [3577 (Ar) and 3566 cm⁻¹ (N₂)]. This does not support (and seems to contradict) the interpretation of the final steps of UV-induced

changes of *N*-hydroxypyridine-2(1*H*)-thione in terms of generation of free hydroxyl radicals separated in the matrix lattice from pyridylthiyl radicals **IV**.

Moreover, if the final products of the photochemical transformations of matrix-isolated *N*-hydroxypyridine-2(1*H*)-thione were hydroxyl radicals and pyridylthiyl radicals **IV**, then the spectra recorded after prolonged exposure of **I** or **DI** to UV ($\lambda > 345$ nm or $\lambda > 295$ nm) light should consist of the spectrum of pyridylthiyl radical **IV** (see Figure S4, in the Supporting Information) and a single band due to the stretching vibration of OH or OD bond. Hence, except for the ν OH and ν OD bands, the spectra of the final photoproducts generated from **I** and from **DI** should be *identical*, regardless whether the compound was deuterated or not. Therefore, the identity (or lack of it) of the spectra (below 2500 cm⁻¹) recorded after prolonged $\lambda > 345$ nm (or $\lambda > 295$ nm) irradiation of **I** and the spectra recorded after analogous irradiation of **DI** should be a very important observation, crucial for the analysis of the photochemical changes of **I**.

The IR spectra of the final products of the UV-induced transformations of **I** and of **DI**, isolated in Ar matrixes, are presented in Figure 4, traces C and D, respectively. It is apparent that most of the bands in these spectra are placed at the same (or very similar) position, regardless of the initial substrate **I** or **DI**. One of the differences, concerning the ν OH and ν OD bands, found, respectively, at 3577 and 2643 cm⁻¹, could be explained in terms of the pair of hydroxyl and pyridylthiyl

radicals isolated separately in a matrix. But the spectra shown in traces C and D of Figure 4 differ also by the positions of other absorptions. One of the pairs of such absorptions appears at the standard position of bands due to in-plane bending vibrations of the OH or OD groups (β OH or β OD). The band in spectrum C was observed at 1169 cm^{-1} , whereas the band in spectrum D was found at 863 cm^{-1} . A second pair of such bands, which can be interpreted as originating from out-of-plane torsions of the OH or OD groups (τ OH or τ OD), appear at 372 cm^{-1} (spectrum C) and 282 cm^{-1} (spectrum D). Comparison of the spectra recorded after prolonged UV ($\lambda > 345\text{ nm}$ or $\lambda > 295\text{ nm}$) irradiation of **I** (Figure 4E) and **DI** (Figure 4F) isolated in N_2 matrixes yields the same picture. Correctness of the assignment of the β OH and τ OH bands (indicated in Figure 4) is supported by their broadening and shift toward higher wavenumbers, when Ar matrix environment was replaced by solid N_2 .

Appearance of the β OH/ β OD as well as τ OH/ τ OD bands (by which the spectra of product(s) generated from **I** differ from the spectra of product(s) generated from **DI**) strongly contradicts the hypothesis that the final products of the photochemical changes of *N*-hydroxypyridine-2(1*H*)-thione could be the $\cdot\text{OH}$ radical and the pyridylthiyl radical **IV**.

In search of an alternative interpretation of the UV-induced transformations of matrix-isolated *N*-hydroxypyridine-2(1*H*)-thione (observed by FTIR spectroscopy), theoretical simulations of infrared spectra have been carried out [at the DFT(B3LYP)/6-311++G(d, p) level], for a number of trial structures of the photoproducts. By this method the final product photogenerated from **I** has been identified as the form **IIIb**. The spectra calculated for this species (as well as for its deuterated isotopologue **DIIIb**) are compared (in Figure 4) with the experimental spectra recorded after prolonged UV ($\lambda > 345\text{ nm}$ or $\lambda > 295\text{ nm}$) irradiation of matrix-isolated **I** or **DI**. The general agreement between the experimental and theoretical spectra is very good. This is true for nondeuterated species **IIIb** as well as for deuterated **DIIIb**. Identity of the experimental spectra of the final products photogenerated from nondeuterated and deuterated precursors (except for the bands due to ν OH/ ν OD, β OH/ β OD, and τ OH/ τ OD) is well reproduced in theoretical simulations. Also the isotope shifts of the ν OH/ ν OD, β OH/ β OD, and τ OH/ τ OD bands are well theoretically predicted. In the structure of **IIIb**, the OH group is not involved in an intramolecular hydrogen bond with the lone electron pair of the nitrogen atom. Hence, in agreement with experimental observation, the IR band due to ν OH vibration is predicted at high wavenumber. The frequencies and integrated intensities of the bands observed in the IR spectra of the final product of the photoinduced transformations of **I** (and **DI**) are collected in Tables S5 and S6 (in the Supporting Information). In these tables the experimental spectra are interpreted by comparison with frequencies, intensities, and normal-mode forms theoretically predicted for **IIIb** and **DIIIb**.

Identification of the final product of photochemical changes of matrix-isolated *N*-hydroxypyridine-2(1*H*)-thione provided also a hint for identification of the intermediate product appearing in the course of UV irradiation of **I**. Following the progress of the UV-induced reaction it was easy to observe that many IR bands in the spectrum of the intermediate photoproduct overlap (or partly overlap) with the bands due to final photoproduct (see Figure S5, in the Supporting Information). These coinciding IR absorptions suggest that the two photogenerated species might have similar structures. This requirement is best fulfilled by form **IIIa** as a candidate for the structure of the

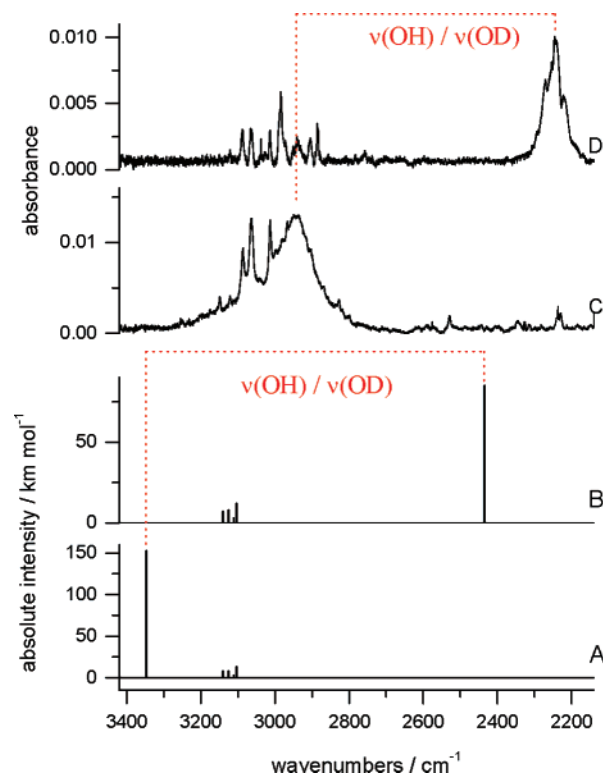


Figure 5. Extracted infrared spectrum of the intermediate photoproduct generated upon UV irradiation of *N*-hydroxypyridine-2(1*H*)-thione isolated in a N_2 matrix (C); extracted infrared spectrum of the intermediate photoproduct generated upon UV irradiation of the deuterated isotopologue of *N*-hydroxypyridine-2(1*H*)-thione isolated in a N_2 matrix (D); infrared spectra calculated at the DFT(B3LYP)/6-311++G(d, p) level for **IIIa** (A) and **DIIIa** (B). The theoretical wavenumbers were scaled by the single factor of 0.98.

intermediate photoproduct. Forms **IIIa** and **IIIb** differ only by a rotation of the OH group with respect to the 2-pyridinethione frame. However, the rotation of the OH has one important consequence: there is an intramolecular hydrogen bond in **IIIa**, but in **IIIb** there are no intramolecular hydrogen bonds. That is why the sharp bands due to stretching vibrations of free OH (or OD) groups were observed in the IR spectra of the final product, whereas in the spectrum of the intermediate product the broad ν OH and ν OD bands were observed at much lower wavenumbers (Figure 5), indicating involvement of the OH and OD groups in a hydrogen bond. Because of the same reason, the presence of the intramolecular hydrogen bonding in **IIIa** and its absence in **IIIb**, also the positions of the bands due to β OH and τ OH are different in the spectra of these two photoproducts (see regions 1350–1250 and 450–350 cm^{-1} in Figure S5 in the Supporting Information). The extracted experimental spectra of the intermediate products photogenerated from **I** or **DI** are well reproduced by the spectra theoretically predicted for structures **IIIa** and **DIIIa**, respectively (see Figure 6). The correctness of the identification of the intermediate product as form **IIIa** as well as the assignment of structure **IIIb** to the final photoproduct is further supported by the fact that the details, by which the experimental spectra of these two photoproducts differ, are very well reproduced by the spectra calculated for **IIIa** and **IIIb** (see Figure 3). The assignment of IR bands observed in the spectra of the intermediate product, appearing during UV irradiation of matrix-isolated **I** or **DI**, to the frequencies and forms of the normal modes calculated for **IIIa** and **DIIIa** is given in Tables S7 and S8, in the Supporting Information.

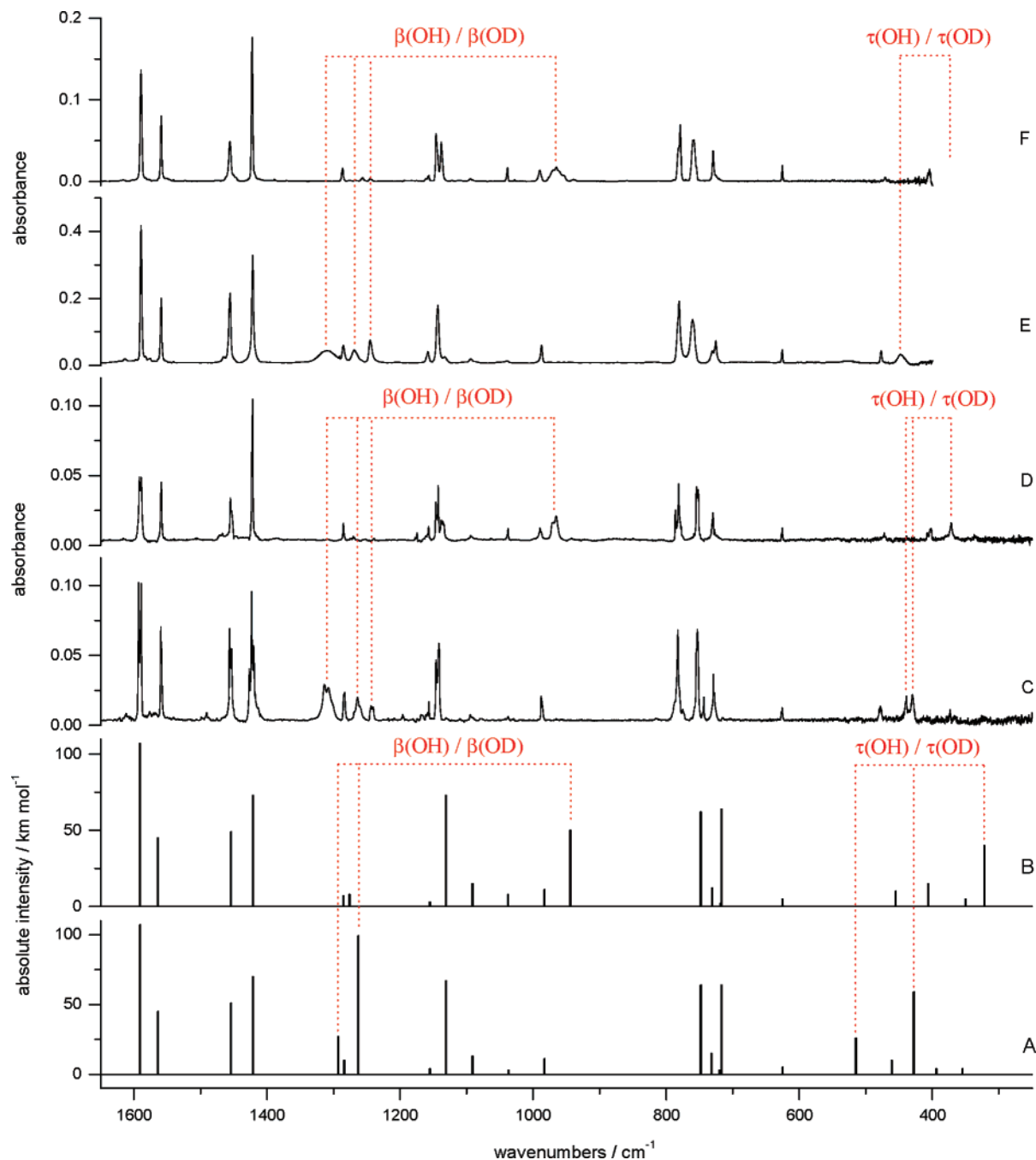


Figure 6. Extracted infrared spectra of the intermediate photoproduct generated upon UV irradiation of *N*-hydroxypyridine-2(1*H*)-thione isolated in an Ar matrix (C) or in a N_2 matrix (E); extracted infrared spectra of the intermediate photoproduct generated upon UV irradiation of the deuterated isotopologue of *N*-hydroxypyridine-2(1*H*)-thione isolated in an Ar matrix (D) or in a N_2 matrix (F); infrared spectra calculated at the DFT(B3LYP)/6-311++G(d, p) level for **IIIa** (A) and **DIIIa** (B). The theoretical wavenumbers were scaled by the single factor of 0.98.

Theoretical Model

The energies of vertical excitations to the lowest singlet states of **I** were calculated, in the present work, with the CC2/aug-cc-pVDZ method at the equilibrium geometry of the ground S_0 state optimized at the MP2/cc-pVDZ level. The obtained values are collected in Table 2, together with the oscillator strengths of the corresponding transitions and the dipole moments of the system in S_1 , S_2 , and S_3 states. The results of analogous calculations carried out for **IIIa** are presented in Table 3. The lowest-energy electronic excitations in **I** arise from π and n orbitals (which are mostly localized on sulfur) to the π^* orbital of the pyridine ring. According to the calculations, the moderately strong ($f = 0.068$) absorption to S_1 (of the ${}^1\pi\pi^*$ character) should appear in the near-UV ($\Delta E = 3.67$ eV), absorption to

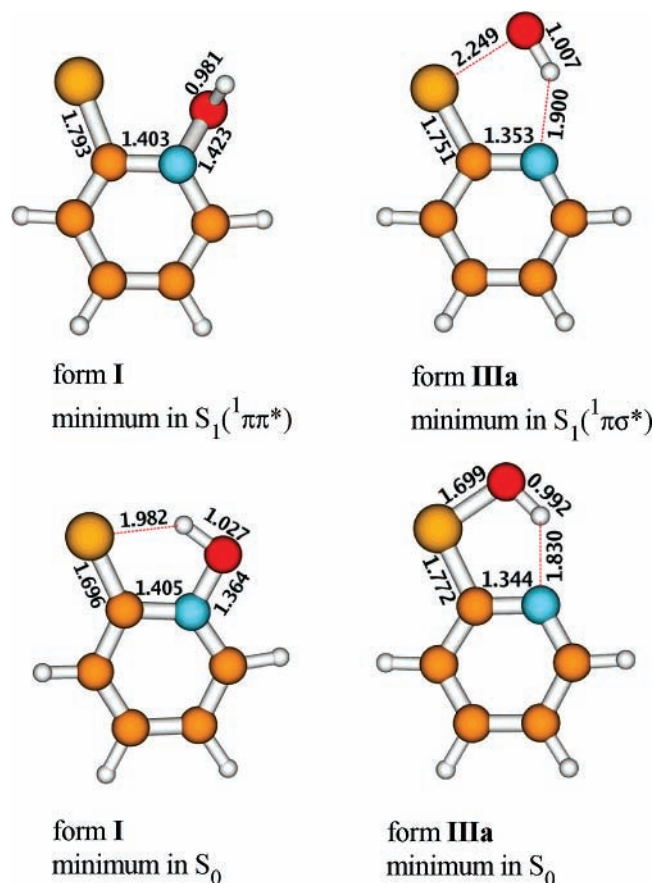
TABLE 2: Vertical Excitation Energies (ΔE), Oscillator Strengths (f), and Dipole Moments (μ) Calculated with the CC2/aug-cc-pVDZ Method at the MP2/cc-pVDZ Equilibrium Geometry of Form I

state	$\Delta E/\text{eV}$	f	μ/Debye
S_0			4.47
${}^1\pi\pi^*$	3.69	0.068	0.32
${}^1n\pi^*$	4.00	5×10^{-4}	2.35
${}^1\pi\pi^*$	4.43	0.325	1.25

the ${}^1n\pi^*$ state S_2 ($\Delta E = 4.00$ eV, $f = 5 \times 10^{-4}$) should be very weak, whereas the absorption to the second ${}^1\pi\pi^*$ state S_3 should be strongly allowed ($\Delta E = 4.43$ eV, $f = 0.325$). Vertical excitation of **I** to the S_1 , S_2 , and S_3 excited states reduces significantly the dipole moment of the system. This effect is

TABLE 3: Vertical Excitation Energies (ΔE), Oscillator Strengths (f), and Dipole Moments (μ) Calculated with the CC2/aug-cc-pVDZ Method at the MP2/cc-pVDZ Equilibrium Geometry of Form IIIa

state	$\Delta E/eV$	f	μ/Debye
S_0			3.97
$^1\pi\sigma^*$	3.82	3×10^{-4}	5.59
$^1\pi\pi^*$	4.12	0.082	2.54
$^1\pi\pi^*$	4.63	0.225	2.90

CHART 2: Geometry of Forms I and IIIa in the Ground (S_0) State (Optimized at the MP2/cc-pVDZ Level) and in the Lowest Excited Electronic (S_1) State (Optimized at the CC2/cc-pVDZ Level)

more pronounced for the $\pi\pi^*$ excitations to the S_1 and S_3 states than for the $n\pi^*$ excitation to the S_2 state (see Table 2).

As can be seen in Table 3, the lowest excited electronic singlet state of **IIIa** has a $\pi\sigma^*$ character. Such a state should have repulsive character, as far as dissociation of the SO single bond is concerned. However, direct population of this S_1 state of **IIIa** by excitation from S_0 with a near-UV photon should be very improbable due to very small oscillator strength $f = 3 \times 10^{-4}$ (see Table 3). The $S_1(^1\pi\sigma^*)$ state of **IIIa** can be populated by a dipole-allowed absorption to $S_2(^1\pi\pi^*)$ followed by internal conversion to S_1 .

The optimized geometries of **I** and **IIIa** in S_0 and S_1 electronic states are presented in Chart 2. The most important geometry parameters, changing significantly upon $S_0 \rightarrow S_1$ excitation, are indicated in this chart. The molecule of **I** is predicted (at the CC2/cc-pVDZ level) to be planar in S_0 , whereas in S_1 the hydroxyl group gets perpendicular to the ring and a considerable pyramidalization appears at the nitrogen atom (with the sum of the bond angles equal to 345°). Electronic excitation disturbs also the lengths of the bonds in the structure **I**, with the most

pronounced changes concerning the C–S ($\Delta R_{CS} = 0.097 \text{ \AA}$) and N–O ($\Delta R_{NO} = 0.059 \text{ \AA}$) bond lengths.

The potential energy (PE) profile calculated along the minimum-energy path (MEP) for detachment of the hydroxyl group in the lowest excited S_1 singlet state of **I** is presented in Figure 7 (solid line). In addition, the PE profile of the S_0 state, calculated along the MEP optimized for the S_1 state, is also shown in this figure (dashed line). Inspection of the results shows that the PE function of the S_1 state is virtually dissociative with respect to detachment of the hydroxyl group (see also refs 39 and 40). On the PE surface of S_1 , the estimated barrier for the OH radical dissociation (ca. 4 kJ mol^{-1} , see Figure 7) is lower than the zero-vibrational-energy level of the system. Near to the top of the barrier, the π^* orbital (terminal for electronic excitation) transforms into the orbital with a significant σ^* antibonding character with respect to N–O. After passing the barrier, the gap between the PE functions of the S_0 and S_1 states diminishes with increasing N–O distance. Finally, at $R_{NO} = 1.8 \text{ \AA}$ the surfaces of the S_0 and S_1 states are very close to each other. Beyond this point, crossing of S_0 and S_1 cannot be well characterized with the aid of the single-reference CC2 method. Nevertheless, crossing of PE surfaces of S_0 and S_1 (a conical intersection of these two states) can be anticipated by extrapolation of the calculated PE profiles, for distances longer than the last converged point at $R_{NO} = 1.8 \text{ \AA}$ (see Figure 7).

Dependence of the potential energy of **IIIa** in S_0 and S_1 states on the S–O distance is presented in the right-hand part of Figure 7. This plot shows that at R_{SO} distances larger than 3.2 \AA the system adopts a structure with only loose bonding between the hydroxyl group and the rest of the molecule. At such a distance the energy of the system in S_0 is very similar to that of the system in S_1 . The plot presented in Figure 7 suggests that there is a conical intersection (CI) between the S_0 and S_1 states and that this CI corresponds to dissociation/association reaction of the hydroxyl group and the pyridylthiyl radical **IV**. The region of this CI is easily accessible by the system excited to S_1 . Moreover, from the strongly nonadiabatic CI region, the system can barrierlessly relax on the S_0 potential energy surface to the ground-state minima of forms **I** and **III**.

Concluding Discussion

Experimental identification of the intermediate and final products (**IIIa** and **IIIb**, respectively) of the UV-induced transformations of matrix-isolated **I**, combined with the results of theoretical calculations of PE surfaces of S_0 and S_1 states of these species, allow proposition of a self-consistent scheme of the observed photoreaction (Scheme 1). In this scheme, the initial step concerns homolytic cleavage of the N–O bond of the *N*-hydroxypyridine-2(1*H*)-thione molecule excited by a near-UV photon. The released hydroxyl radical $\cdot\text{OH}$ can be easily trapped, especially in a cage of a low-temperature matrix, by the sulfur atom of the pyridylthiyl radical **IV**. This recombination of the radicals yields a new compound 2-hydroxysulfanylpyridine **III**, which can adopt two rotameric structures **IIIa** and **IIIb**. As follows from experimental observations, breaking of the intramolecular hydrogen bond in **IIIa** and generation of **IIIb** requires some excess of the excitation energy. That is why for photogeneration of this latter form irradiation of the matrixes with shorter-wavelength UV light was necessary.

Supporting Information Available: Chart S1 showing the atom numbering for *N*-hydroxypyridine-2(1*H*)-thione (**I**) and 2-hydroxysulfanylpyridine (**III**); Table S1 with the relative energies of *N*-hydroxypyridine-2(1*H*)-thione isomers; Table S2

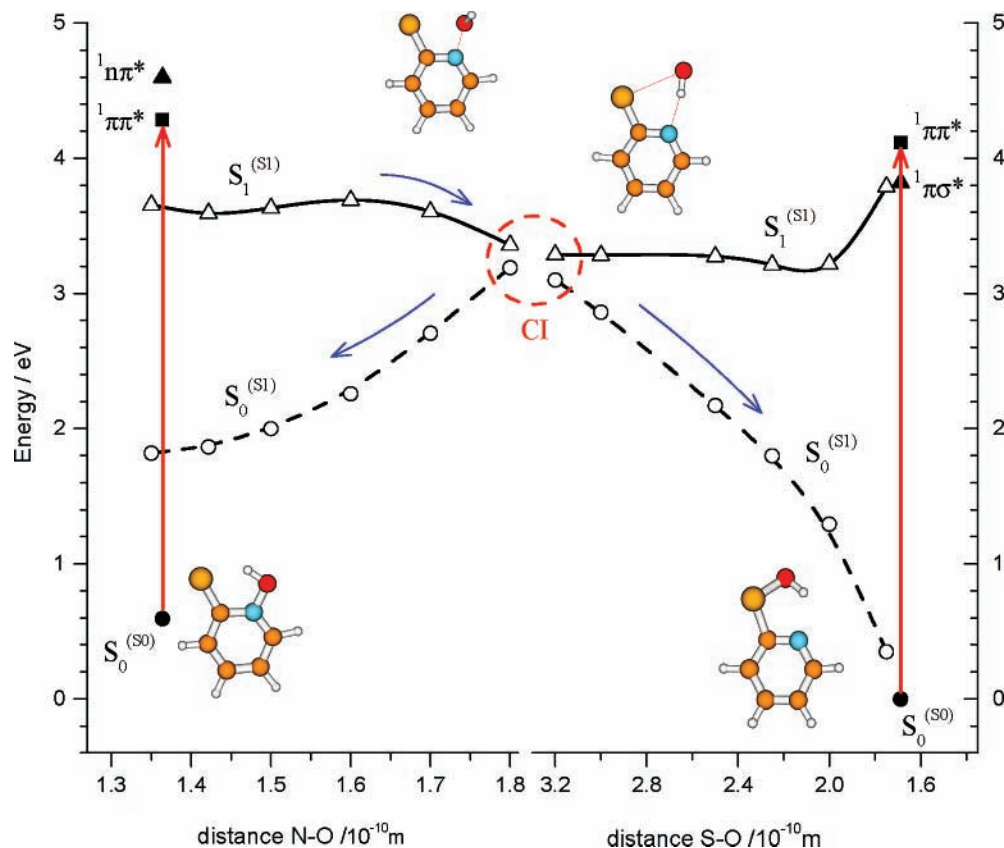
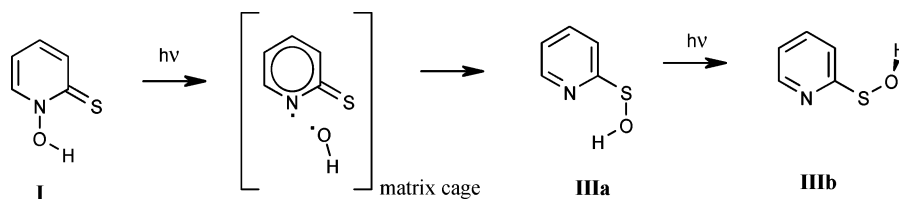


Figure 7. Potential energy profiles of the S_0 state (circles) and the lowest excited singlet state S_1 (triangles) calculated for structures **I** (left) and **IIIa** (right) as functions of N–O and S–O distances, respectively. Solid lines: minimum-energy-path profiles in the lowest excited singlet state ($S_1^{(S1)}$). Dashed lines: profiles of the energy of the ground electronic state calculated at the geometry of the S_1 state ($S_0^{(S1)}$).

SCHEME 1: Phototransformations of Monomeric *N*-Hydroxypyridine-2(1*H*)-thione Isolated in Low-Temperature Ar or N_2 Matrixes



providing definitions of the internal coordinates used in the normal-mode analysis carried out for the isomers of *N*-hydroxypyridine-2(1*H*)-thione; Tables S3–S8 providing the experimental and theoretical [DFT(B3LYP)/6-311++G(d, p)] wavenumbers and intensities of the bands in the IR spectra of *N*-hydroxypyridine-2(1*H*)-thione (**I**), its deuterated isotopologue (**DI**), and the (**IIIa**) and (**IIIb**) rotamers of 2-hydroxysulfanylpyridine and their deuterated isotopologues (**DIIIa**), (**DIIIb**); Figures S1 and S2 showing the comparison of experimental spectra of *N*-hydroxypyridine-2(1*H*)-thione (**I**) and its deuterated isotopologue (**DI**), isolated in Ar and N_2 matrixes, with the results of theoretical calculations carried out for **I**, **DI** as well as for 2-mercaptopyridine *N*-oxide (**II**); Figure S3 showing the comparison of the high-frequency range of the IR spectra recorded during the progress of UV-induced transformations of **I** with the spectra calculated for **I**, **IIIa**, and **IIIb**; Figures S4 and S5 showing the comparison of the experimental IR spectra of the final and the intermediate products generated upon UV irradiation of **I** with the spectra theoretically predicted for **IIIa**, **IIIb**, and **IV**. This material is available free of charge via the Internet at <http://pubs.acs.org>.

References and Notes

- (1) Evans, P. G. E.; Sudgen, J. K.; van Abbe, N. *J. Pharm. Acta Helv.* **1975**, *50*, 94.
- (2) Neihof, R. A.; Bailey, C. A.; Patouillet, C.; Hannan, P. J. *Arch. Environ. Contam. Toxicol.* **1979**, *8*, 355.
- (3) Barnett, B. L.; Kretshmar, H. C.; Hartman, F. A. *Inorg. Chem.* **1977**, *16*, 1834.
- (4) Blatt, J.; Taylor, S. R.; Kontoghiorghes, G. J. *Cancer. Res.* **1989**, *49*, 2925.
- (5) Burrows, C. J.; Muller, J. G. *Chem. Rev.* **1998**, *98*, 1109.
- (6) Cadet, J.; Sage, E.; Douki, T. *Mutat. Res.* **2005**, *571*, 3.
- (7) Cadet, J.; Berger, M.; Douki, T.; Ravanat, J.-L. *Mutat. Res.* **2003**, *531*, 5.
- (8) Pelle, E.; Huang, X.; Mammone, T.; Marenus, K.; Maes, D.; Frenkel, K. *J. Invest. Dermatol.* **2003**, *121*, 177.
- (9) Walling, C. *Acc. Chem. Res.* **1975**, *8*, 125.
- (10) Epe, B.; Ballmaier, D.; Adam, W.; Grimm, G. N.; Saha-Möller, C. *R. Nucleic Acids Res.* **1996**, *24*, 1625.
- (11) Chaulk, S. G.; Pezacki, J. P.; MacMillan, A. M. *Biochemistry* **2000**, *39*, 10448.
- (12) Tobin, D.; Arvanitidis, M.; Bisby, R. H. *Biochem. Biophys. Res. Commun.* **2002**, *299*, 155.
- (13) Adam, W.; Ballmaier, D.; Epe, B.; Grimm, G. N.; Saha-Möller, C. *R. Angew. Chem., Int. Ed. Engl.* **1995**, *34*, 2156.
- (14) Aveline, B. M.; Kochevar, I. E.; Redmond, R. W. *J. Am. Chem. Soc.* **1996**, *118*, 10113.

- (15) Aveline, B. M.; Kochevar, I. E.; Redmond, R. W. *J. Am. Chem. Soc.* **1996**, *118*, 289.
- (16) Aveline, B. M.; Kochevar, I. E.; Redmond, R. W. *J. Am. Chem. Soc.* **1996**, *118*, 10124.
- (17) Møller, C.; Plesset, M. S. *Phys. Rev.* **1934**, *46*, 618.
- (18) Becke, A. *Phys. Rev. A* **1988**, *38*, 3098.
- (19) Lee, C. T.; Yang, W. T.; Parr, R. G. *Phys. Rev. B* **1988**, *37*, 785.
- (20) Pople, J. A.; Head-Gordon, M.; Raghavachari, K. *J. Chem. Phys.* **1987**, *87*, 5968.
- (21) Frisch, M. J.; Trucks, G. W.; Schlegel, H. B.; Scuseria, G. E.; Robb, M. A.; Cheeseman, J. R.; Montgomery, J. A., Jr.; Vreven, T.; Kudin, K. N.; Burant, J. C.; Millam, J. M.; Iyengar, S. S.; Tomasi, J.; Barone, V.; Mennucci, B.; Cossi, M.; Scalmani, G.; Rega, N.; Petersson, G. A.; Nakatsuji, H.; Hada, M.; Ehara, M.; Toyota, K.; Fukuda, R.; Hasegawa, J.; Ishida, M.; Nakajima, T.; Honda, Y.; Kitao, O.; Nakai, H.; Klene, M.; Li, X.; Knox, J. E.; Hratchian, H. P.; Cross, J. B.; Adamo, C.; Jaramillo, J.; Gomperts, R.; Stratmann, R. E.; Yazyev, O.; Austin, A. J.; Cammi, R.; Pomelli, C.; Ochterski, J. W.; Ayala, P. Y.; Morokuma, K.; Voth, G. A.; Salvador, P.; Dannenberg, J. J.; Zakrzewski, V. G.; Dapprich, S.; Daniels, A. D.; Strain, M. C.; Farkas, O.; Malick, D. K.; Rabuck, A. D.; Raghavachari, K.; Foresman, J. B.; Ortiz, J. V.; Cui, Q.; Baboul, A. G.; Clifford, S.; Cioslowski, J.; Stefanov, B. B.; Liu, G.; Liashenko, A.; Piskorz, P.; Komaromi, I.; Martin, R. L.; Fox, D. J.; Keith, T.; Al-Laham, M. A.; Peng, C. Y.; Nanayakkara, A.; Challacombe, M.; Gill, P. M. W.; Johnson, B.; Chen, W.; Wong, M. W.; Gonzalez, C.; Pople, J. A. *Gaussian 03*, revision C.02.; Gaussian, Inc.: Wallingford, CT, 2004.
- (22) Schachtschneider, J. H. *Vibrational Analysis of Polyatomic Molecules, Parts V and VI*; Technical Report; Shell Development Co.: Emeryville, CA, 1964 and 1965.
- (23) Pulay, P.; Fogarasi, G.; Pang, F.; Boggs, J. E. *J. Am. Chem. Soc.* **1979**, *101*, 2550.
- (24) Keresztury, G.; Jalsovszky, G. *J. Mol. Struct.* **1971**, *10*, 304.
- (25) Hättig, C.; Weigend, F. *J. Chem. Phys.* **2000**, *113*, 5154.
- (26) Ahlrichs, R.; Bär, M.; Häser, M.; Horn, H.; Kölmel, C. *Chem. Phys. Lett.* **1989**, *162*, 165.
- (27) Woon, D. E.; Dunning, T. H., Jr. *J. Chem. Phys.* **1993**, *98*, 1358.
- (28) Hättig, C. *J. Chem. Phys.* **2003**, *118*, 7751.
- (29) Köhn, A.; Hättig, C. *J. Chem. Phys.* **2003**, *119*, 5021.
- (30) Schaefer, A.; Horn, H.; Ahlrichs, R. *J. Chem. Phys.* **1992**, *97*, 2571.
- (31) Bond, A.; Jones, W. *Acta Crystallogr., Sect. C* **1999**, *55*, 1536.
- (32) Rostkowska, H.; Nowak, M. J.; Lapinski, L.; Adamowicz, L. *Phys. Chem. Chem. Phys.* **2001**, *3*, 3012.
- (33) Rostkowska, H.; Lapinski, L.; Nowak, M. J.; Adamowicz, L. *Int. J. Quantum Chem.* **2002**, *90*, 1163.
- (34) Khriachtchev, L.; Pettersson, M.; Tuominen, S.; Rasanen, M. *J. Chem. Phys.* **1997**, *107*, 7252.
- (35) Engdahl, A.; Karlstrom, G.; Nelander, B. *J. Chem. Phys.* **2003**, *118*, 7797.
- (36) Mielke, Z.; Olbert-Majkut, A.; Tokhadze, K. G. *J. Chem. Phys.* **2003**, *118*, 1364.
- (37) Olbert-Majkut, A.; Mielke, Z.; Tokhadze, K. G. *J. Mol. Struct.* **2003**, *665*, 321.
- (38) Cheng, B.-M.; Lee, Y.-P.; Ogilvie, J. F. *Chem. Phys. Lett.* **1988**, *151*, 109.
- (39) Arnone, M.; Engels, B. *J. Phys. Chem. A* **2006**, *110*, 12330.
- (40) Arnone, M.; Hartung, J.; Engels, B. *J. Phys. Chem. A* **2005**, *109*, 5943.